Desalination and Water Treatment
www.deswater.com
doi: 10.1080/19443994.2015.1032362

57 (2016) 9957–9970
May

Taylor & Francis
Taylor & Francis Group

Nanostructured activated carbon xerogels for removal of methomyl pesticide

Nady A. Fathy[a,*], Amina A. Attia[a,*], Bahira Hegazi[b]

[a]*Physical Chemistry Department, National Research Centre, 12622 El-Behouth St., El-Dokki, Giza, Egypt, Tel. +20 2 33371433; Fax: +20 2 33370597; emails: fathyna.77@hotmail.com (N.A. Fathy), amina_abdelmeguid@yahoo.com (A.A. Attia)*
[b]*Applied Organic Chemistry Department, National Research Centre, 12622 El-Behouth St., El-Dokki, Giza, Egypt, email: nrc_byh@yahoo.com*

Received 16 October 2014; Accepted 17 March 2015

ABSTRACT

Three nanoporous activated carbon xerogels were synthesized by chemical activation of resorcinol–formaldehyde xerogel (RFX) with activating agents such as monoethanol amine (CX-MEA), phosphoric acid (CX-HPO), and potassium hydroxide (CX-KOH), respectively. The effect of activating agents on the internal porosity, structure, and surface functional groups was investigated using N_2 gas adsorption–desorption, FTIR, scanning electron microscopy/energy dispersive X-ray analyzer, and TEM techniques. High values of surface area and total pore volume of 1,146 and 1,700 m^2/g, 0.9446 and 1.668 cm^3/g were found in the carbon xerogels CX-HPO and CX-KOH, respectively. The capacity of the produced carbons to remove the methomyl pesticide by adsorption from aqueous solution was explored. It was found that the adsorption capacity increased sharply with the increase in the surface area and mesopore volume. Equilibrium adsorption data were analyzed by Langmuir, Freundlich, and Temkin isotherm models. The batch studies were best fitted to Langmuir and Temkin isotherms, attaining a maximum adsorption capacity (Q_m = 125 mg/g) of methomyl onto CX-KOH. Adsorption kinetic studies were employed and the adsorption process was found to follow the pseudo-second-order kinetic model. The values of calculated Gibbs free energy (ΔG°) showed that the adsorption of methomyl is a feasible, spontaneous, and endothermic process.

Keywords: Nanostructured materials; Activated carbon xerogels; Surface characteristics; Adsorption; Methomyl pesticide

1. Introduction

Pollution and water scarcity along with climate changes are the most intricate environmental turmoils for the twenty-first century [1]. Pollution of surface and groundwater causes risks to aquatic organisms and human health. For example, pesticides worldwide are used to prevent crops, forestry, and horticultural from the damages of insects, diseases, and other pests, to adjust the growth of the plants and to increase the yields of the crops. However, only a small part of the applied pesticides reaches its final destination and the biological targets. The residual pesticides are still toxicologically active, leading to the contamination of soil and groundwater [2,3]. This contamination arises from surface runoff, leaching, wind erosion, deposition from aerial applications, industrial discharges, and various other sources [4].

*Corresponding authors.

Among the most commonly used pesticides, the methomyl (IUPAC name is *S-methyl N-(methylcarbamoyloxy) thioacetimidate*) stands for the top-ranking sales among oxime carbamates due to its use in a wide variety of applications in agricultural, including vegetable, arthropods on various field crops, sod farms, livestock quarters, and commercial ornamentals [5] as it is registered to use as an aerial dispersant [6]. Methomyl is highly soluble in water (58 g/L at 25˚C) and is moderately persistent. In water, it is stable under neutral to acidic pH ranges, but it degrades in alkaline conditions into *S-methyl N-hydroxy thioacetimidate* and *methomyl oxime* which may be further degraded to acetonitrile and carbon dioxide [7]. It can contaminate surface water from spray drift during application or by runoff from treated sites. It has been detected frequently in surface and groundwater in monitoring studies at concentrations typically below 1 μg/L [6–9]. Therefore, it is important to develop remediation technologies for methomyl-contaminated water which is necessary for public health and safety point of view.

A wide variety of treatment technologies for the removal of pesticides, e.g. methomyl, have been studied such as precipitation, coagulation–flocculation, sedimentation, flotation, filtration, membrane processes, electrochemical techniques, biological process, chemical reaction, ion exchange, and adsorption [4,8–16]. Among of these processes, adsorption onto porous adsorbents is recognized as the most efficient and promising fundamental approach in the wastewater treatment processes [13]. To the best of our knowledge, only a few studies have been carried out on the removal of methomyl pesticide onto polymeric materials and activated carbons [4,14–16]. Accordingly, the adsorption studies of methomyl using activated carbon xerogels (ACXs) as adsorbents have not been investigated to date.

Carbon xerogels belong to a new class of technical-grade carbon, which has continuously attracted the attention of specialists in catalysis over the past decade. The increased interest in these carbon materials is due to their unique structure and properties, which are better than those of other carbon materials applicable as sorbents and catalyst supports [17,18]. They possess high surface area, high porosity, open pore network, and controllable pore size, and can be prepared in the desired forms (e.g. monoliths, thin films, or powders). Accordingly, the combination of these properties gained carbon xerogels the perfect candidates for diverse applications such as supercapacitors, fuel cells, separation, desalination systems, and catalyst supports [18–20]. Recently, ACXs have attracted a great attention of interest due to their textural properties can be tailored with different pore sizes of micro, meso, and macropores. Hence, they are more adequate for liquid-phase applications [18,20,21] with a low-cost production as compared to other carbon gels.

Furthermore, the chemical activation is one of the most popular routes to produce nanoporous ACXs in order to increase their surface functionalities and textural properties, and consequently improving their adsorption and ion exchange characteristics toward various adsorbents as well as their catalytic selectivity. Particularly, the chemical activation of resorcinol–formaldehyde xerogels (RFXs) with activating agents of H_3PO_4, K_2CO_3, KOH, and NaOH has been carried out [18–24]. Elsayed et al. [25] used monoethanol amine (MEA) as a catalyst in the polycondensation of resorcinol–formaldehyde, but in our study, MEA was employed as a new chemical agent to activate the RFX.

Therefore, the objectives of the present work were to explore: (i) the impact of various chemical agents on the textural and surface characteristics of the nanoporous ACX produced from activation of RFX with monoethanol amine, phosphoric acid, and potassium hydroxide; (ii) the feasibility of the produced carbons as porous adsorbents for the adsorption of methomyl pesticide from aqueous solution; (iii) the influence of factors such as pH of methomyl solution, carbon dose, and temperature on adsorption behavior of methomyl onto the prepared carbons; and (iv) the equilibrium and kinetic adsorption data of methomyl using Langmuir, Freundlich, and Temkin models as well as adsorption mechanisms employing pseudo-first-order, pseudo-second-order, and intraparticle diffusion kinetic models in this investigation.

2. Materials and methods

2.1. Synthesis of RFX

RFX was synthesized by the polycondensation of R ($C_6H_4(OH)_2$, Panreac, 99%) and F (HCHO, Aldrich, 36–38%), stabilized by 10–15% methanol (CH_3OH, Aldrich, 99%) in the presence of potassium carbonate (K_2CO_3, POCH SA, 99%) as alkaline catalyst (C). Distilled water was used as the solvent. The molar ratios of R/F and R/C were fixed at 0.5 and 1,000, respectively, and pH of the sol was adjusted to 6. The prepared mixture (sol) was then stirred at 90˚C for 60 min until the hydrogel is formed. The obtained hydrogel was transferred into a stoppered glass bottle to cool and then left at room temperature for 3 d to complete curing and gelling process. The hydrogel was placed in acetone solvent to exchange with water in an open beaker for one day. The produced aceto-gel was heated slowly in an air-oven at 90˚C and held

for 12 h, being finally heated at 110˚C for 120 min to get the organic RFX.

2.2. Synthesis of ACXs

Three different chemical activation schemes using monoethanol amine (MEA, $NH_2CH_2CH_2OH$, Panreac, 99%), phosphoric acid (H_3PO_4, ABCO CHEMIE, 85%), and potassium hydroxide (KOH, Modern Lab, 99%) as activating agents were adopted on the as-prepared RFX.

In the first process, the RFX was chemically activated with monoethanol amine as follows. The RFX was mixed with MEA using a mass ratio of 1:1 (MEA/RFX) and left at room temperature overnight. Then, the mixture was pyrolyzed in an electric muffle at 500˚C (using a heating rate of 10˚C/min) for 90 min under its own atmosphere (i.e. generated gases during pyrolysis of RFX). Secondly, the RFX was impregnated with 50% (v/v) H_3PO_4 and kept at room temperature overnight, then pyrolyzed in an electric muffle at 500˚C (using a heating rate of 10˚C/min) for 90 min under its own atmosphere also. The resulting cooled products from MEA and H_3PO_4 activation processes were mixed firstly with 1 M HNO_3 at 50˚C for 60 min under stirring in order to enhance oxygen functional groups and then washed thoroughly with hot distilled water until the pH of the drained solution reached ~6, and finally dried in an air-oven at 110˚C overnight. The products, thus, obtained were denoted as CX-MEA and CX-HPO, respectively.

The third sample of organic RFX was subjected to KOH activation using a mass ratio of 1:1 (KOH/RFX), where KOH was dissolved in a small amount of distilled water. The mixture of RFX and KOH was kept at room temperature overnight and then followed by pyrolysis in an electric muffle at 800˚C (heating rate of 10˚C/min) for 60 min under no external gas flow (its own atmosphere). The obtained product was subsequently washed with 1 M HCl solution to remove unreacted potassium hydroxide or carbonated, then subjected to thorough washing with hot distilled water to neutral filtrate and then dried in an air-oven at 110˚C overnight. The obtained sample was labeled as CX-KOH.

All ACX samples were stored in sealed bottles for further experiments. In addition, these materials were subjected to some measurements of carbon yield, pH of the slurry (pH_{slurry}), methylene blue number, total acidity and basicity, and chemical compositions by scanning electron microscopy (SEM) combined with energy dispersive X-ray (EDX) spectroscopy in order to determine their surface characteristics.

2.3. Characterization of the produced ACXs

The pH values of the slurry of the finely powdered ACXs were measured by contacting 0.01 g of sample with 25 mL distilled water, under stirring at 80˚C for 30 min, and then cooled to record pH of the supernatant liquid using a pH meter (HANNA pH20).

The determination of methylene blue number was carried out by contacting 0.025 g of finely powdered carbon samples with 25 mL of 100 mg/L methylene blue solution under shaking (K-O330-Pro SCILOGEX shaker) for 48 h. The residual concentration of dye was measured at λ_{max} = 664 nm.

The amounts of total acidity and basicity (mmol/g) were determined by immersing 0.1 g of the sample in 100 mL of 0.1 M NaOH or HCl solution in stoppered glass bottles and then shaken for 24 h at room temperature. The excess base and acid of the filtered solutions (10 mL) were titrated with 0.1 M HCl and NaOH, respectively, as reported earlier by Boehm [26]. The number of acid sites (acidity) and the number of basic sites (basicity) were calculated from the amount of HCl and NaOH consumed among the titration, respectively.

SEM combined with EDX spectroscopy analyses was made on JEOL (JXA-840A Electron Probe Microanalyzer, INCAx-sight, Oxford) to determine the morphology and chemical compositions of the specimens. Also, transmission electron microscopy (JEOL, TEM-1230 Electron Analyzer) was used to identify the distribution and size of particles.

The presence of oxygen functional groups on the surface of ACXs was quantitatively determined by Fourier transform infrared spectroscopy (FTIR-6100 JASCO, USA) recorded within the wavenumber 4,000–400 cm^{-1}.

The prepared carbons were characterized texturally and morphologically in order to assess their surface and adsorption properties. Nitrogen adsorption–desorption studies provide information on the textural properties such as specific surface area, pore volume, and pore size distributions (PSDs) of the produced carbon materials. For this purpose, the textural features of the obtained carbons were determined by means of nitrogen physisorption at −196˚C (Quantachrome NOVA Automated Gas Sorption system version 1.12). Prior to nitrogen adsorption–desorption analysis, the sample was degassed at 300˚C for several hours under a vacuum, and the isotherms were measured in the relative pressure (P/P^0) range of 0.01–0.99. The specific surface area, total pore volume, and PSDs were estimated from N_2 adsorption–desorption isotherms applying the Brunauer–Emmett–Teller (BET) and *t*-plot methods [27,28]. The BET analysis was employed for

relative pressure between 0.06 and 0.3 to deduce the specific surface area (S_{BET}, m^2/g), and the total pore volume (V_T, cm^3/g) was calculated from the amount of vapor adsorbed at $P/P^0 = 0.975$. Harkins–Jura equation (*t*-plot) [28] was used to determine the specific external surface area (S_{ext}, m^2/g) and the specific micropore volume (V_{micro}, cm^3/g). The micropore surface area was calculated from the difference between S_{BET} and S_{ext} ($S_{micro} = S_{BET} - S_{ext}$), whereas the mesopore volume was deduced from $(V_{mes}) = V_P - V_o^{\alpha}$, assuming negligible volume due to macropores. The mean pore width (W_{mean}, Å) was calculated from $(2V_T/S_{BET}) \times 10^4$. The PSDs in the prepared samples were determined using the density functional theory (DFT) which assumed a slit-shaped pore [29].

2.4. Adsorption studies of methomyl

To assess the adsorption capacity of the as-prepared carbons for removing methomyl as a model pesticide (MW = 162.2 g/mol, $C_5H_{10}N_2O_2S$), the batch experiments were undertaken at room temperature of 25°C for 24 h. The chemical structure of methomyl is presented in Fig. 1. A pure methomyl stock solution of 1,000 mg/L was prepared by dissolving 1 g in 1 L of distilled water, and then preserved in the refrigerator for subsequent adsorption experiments. Initial concentrations of 10, 20, 50, 80, and 100 mg/L from methomyl were prepared by a proper dilution of the stock solution. The equilibrium adsorption studies were performed by shaking 50 ml of known initial concentrations of methomyl with 0.1 g of finely powdered ACXs (particle size <1 mm) in 100 mL conical flaks at an optimum pH 5 as described in this work.

The effect of the initial pH value of the solution (from 2 to 8) on the removal of methomyl was studied by mixing 50 mL of 100 mg/L methomyl solution with 0.1 g of adsorbent sample in various flasks of different pH values at 25°C. The required pH value was adjusted by drop-wise addition of 0.1 M of NaOH or HCl solution and recorded using a pH meter. The flasks were then covered with rubber caps and placed on a shaker at a fixed agitation speed of 200 rpm for 120 min.

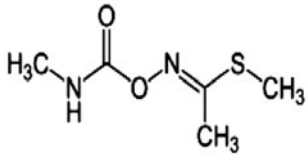

Fig. 1. Chemical structure of methomyl.

In addition, the effect of carbon dose (mg/mL) was studied by contacting 0.02, 0.05, 0.1, 0.2, and 0.5 g per 50 mL of 100 mg/L methomyl solution and then followed by shaking at 200 rpm for 120 min.

The kinetic studies of methomyl adsorbed onto the prepared carbons were investigated by withdrawing aliquots of the solution containing 100 mg/L methomyl (0.2 g adsorbent/100 mL) after desired contact time (5–120 min) and then measuring the absorbance of its residual concentration in the aqueous solution.

The concentrations of methomyl before and after adsorption were determined using UV–vis spectrophotometer (Shimadzu 2401PC) at a maximum wavelength of 233 nm. The amounts of methomyl adsorbed at equilibrium (q_e, mg/g) and at time (q_t, mg/g) were calculated using Eqs. (1) and (2) as follows:

$$q_e = \frac{(C_0 - C_e)}{m} V \tag{1}$$

$$q_t = \frac{(C_0 - C_t)}{m} V \tag{2}$$

where C_0, C_e, and C_t are the liquid-phase concentrations (mg/L) of methomyl at initial, equilibrium, and time, respectively. V is the volume of solution (L) and m is the mass of dried ACXs (g). All the absorbance measurements were performed in triplicate runs. It was found that the relative standard deviations are about ±3%.

3. Results and discussion

In the reported literature devoted to adsorption, the surface area, pore volume, PSD, and surface chemistry are the finger prints of porous carbon adsorbents, in addition to the nature and functional groups of the adsorbate and the solution characteristics (e.g. pH and temperature). These parameters such as pH of the slurry, total acidity, total basicity, and textural properties of the obtained carbons (*cf.* Tables 1 and 2) were taken into account to select the appropriate activation conditions that deserve further investigation of corresponding surface chemistry and methomyl adsorption behavior.

3.1. Physicochemical characteristics

Table 1 presents different physicochemical characteristics of the tested activated carbons. It was found that the carbon yields, after chemical activation, were 10.3, 28.2, and 32.7% for CX-KOH, CX-MEA, and CX-HPO, respectively.

Table 1
Physicochemical properties of the synthesized ACXs

Samples	Density[a] of ACX (g/cm^3)	Carbon[b] yield (%)	pH of the slurry	Methylene blue number (mg/g)	Total acidity (mmol/g)	Total basicity (mmol/g)	% Atomic by EDX analysis				
							C	O	N	P	K
CX-MEA	2.25	28.2	4.66	86.9	2.28	1.12	77.4	19.7	2.82	Nil	Nil
CX-HPO	2.15	32.7	3.84	200	2.59	0.911	86.4	11.3	Nil	1.36	Nil
CX-KOH	2.15	10.3	8.65	215	0.350	3.15	88.6	11.0	Nil	Nil	0.19

[a]Density of carbon is given in the report of adsorption–desorption of N_2 analysis.

[b]Carbon yield is calculated from $= \frac{\text{Weight of activated carbon xerogel}}{\text{Weight of the parent RFX}} \times 100$.

Table 2
Porosity characteristics of the prepared ACXs

Samples	BET-plot			*t*-plot					
	S_{BET} (m^2/g)	V_T (cm^3/g)	W_{mean} (Å)	V_{micro} (cm^3/g)	S_{ext} (m^2/g)	S_{micro} (m^2/g)	V_{meso} (cm^3/g)	S_{micro}/S_{BET} (%)	V_{micro}/V_T (%)
CX-MEA	212.2	0.2236	21.1	0.0155	134.1	78.1	0.2081	36.8	6.93
CX-HPO	1,146	0.9446	16.5	0.3867	397.2	748.8	0.5579	65.4	40.9
CX-KOH	1,700	1.668	19.6	0.4380	723.5	976.5	1.230	57.5	26.3

The pH of the slurry of the prepared carbons recorded in the range of 3.84 (acidic character for CX-HPO) and 8.65 (basic character for CX-KOH) which is in accordance with their total acidities and basicities. For example, the basic character of CX-KOH sample may be related to the presence of oxygen-containing species such as ketonics, pyronics, chromenics, and delocalized π electrons of carbon basal planes [30,31], whereas the acidic character in CX-HPO is owing to the acid oxygen-containing functional groups such as carboxylics, lactonics, and phenolics which could be confirmed by FTIR spectra (Fig. 2). Generally, the pH of the slurry of the tested carbons described the nature of oxygen-containing functional groups located on their surfaces (i.e. acidic or basic oxygen groups). Regarding methylene blue number test, it was found that the methylene blue number increases in the order CX-MEA < CX-HPO < CX-KOH. This result shows that the CX-KOH exhibited the highest methylene blue number (215 mg/g) as compared to the other samples, due to its high surface area and the presence of basic functional oxygen groups as given in Tables 1 and 2.

The elemental compositions of the tested carbons using EDX investigation are depicted in Table 1. It can be seen that these carbons have high carbon and oxygen contents which varied from 77.4 to 88.6% and from 19.7 to 11.0%, respectively. During the carbonization of RFX treated with the chemical agents used, the

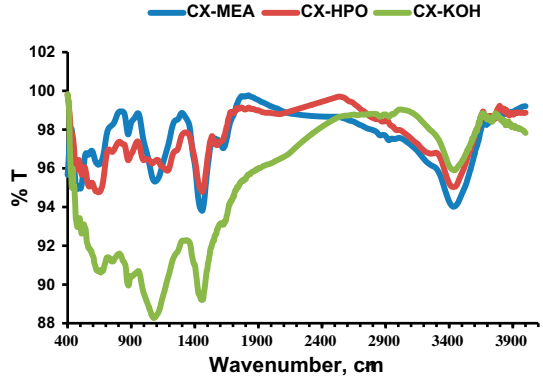

Fig. 2. FTIR spectra of the synthesized ACXs.

O- and H-elements are liberated as small molecules such as water, alcohols, ketones, and acids which revealed as an additional loss in carbon yield and thus enhanced carbon matrix in the resulting carbons. Also, the EDX analysis showed the presence of N-, P-, and K-elements, which attributed to the chemical agent used in the activation process.

3.2. Surface functional groups of the prepared ACXs

Fig. 2 shows the FTIR spectra of ACXs in order to explain the fundamental functional groups which

persist on the carbon surface. These spectra showed the same bands with differences in their intensities to some extent. The broader bands, appearing between 3,780 and 3,300 cm^{-1} within all obtained samples, ascribed to the bending vibrations of adsorbed molecular water and stretching vibrations of –NH and –OH groups, respectively, but it is also strongly associated with stretching vibration of N–H group as observed at 3,430 cm^{-1} in the case of CX-MEA [32]. This confirms the presence of nitrogen functional groups such as amides and amines incorporated in the structure of carbon xerogels which is consistent with EDX analysis (Table 1). Also, it is interesting to observe that the development of aromatic structures can be established from the decrease in intensity of this band as depicted in the FTIR of CX-KOH [33].

An additional band observed at 1,625 cm^{-1} for CX-MEA and CX-HPO could be assigned to conjugated C=O stretching vibration and becomes strongly in CX-MEA which is associated to the C=N stretching vibration in pyridine and amide structures [34]. A strong band at 1,450 cm^{-1} on the CX-(MEA, HPO, and KOH) is assigned to C=C stretching vibration in aromatic rings. The sharp band at 1,098 cm^{-1} is ascribed to C–O and C–O–C skeletal vibrations in ethers, esters, hydroxyls, and phenol groups. However, this band may overlap with the presence of a phosphate ester groups at 1,203 cm^{-1} which is attributed to hydrogen bonded P=O in phosphate ester, to O–C bond in P–O–C (aromatic) linkage, and to P=OOH [35] as only shown in the FTIR of CX-HPO sample. The absorption bands between 1,300 and 900 cm^{-1} have been attributed to C–O single bonds stretching in ethers, phenols, and hydroxyl groups [35]. In addition, the appearance of absorption bands below 900 cm^{-1} has been attributed to out-of-plane vibration of C–H moieties of aromatic structure. Finally, the results highlighted that chemical activation with the performed chemical agents created highly active sites containing oxygen surface functional groups on the prepared carbons which are involved in the adsorption processes.

3.3. Morphological observations of the prepared samples

Scanning electron micrographs (SEM) of the external structures of porous carbons prepared using chemical activation are shown in Fig. 3. It can be seen that the chemical activation with MEA, H_3PO_4, and KOH yielded porous ACXs with roughness and irregular structures, but mostly with varying extents in the shape and distribution of pores (or cavities) which resulted from the shrinkage and compaction on the carbon surface (CX-HPO or CX-KOH), producing high internal porosity. This indicates that the pore development occurred inside the cavities between spherical particles. In order to describe the adsorption process of methomyl onto the prepared carbons, for example, Fig. 3(d) shows the adsorption of methomyl molecules onto CX-HPO sample comparing to Fig. 3(b) for CX-HPO before adsorption. It was observed that the methomyl molecules adsorbed on the entire external surface forming a thin layer adsorption as reported in the section of adsorption studies.

Moreover, TEM photographs of the parent RFX and of the prepared carbon xerogels under consideration are shown in Fig. 4. It is interesting to note that

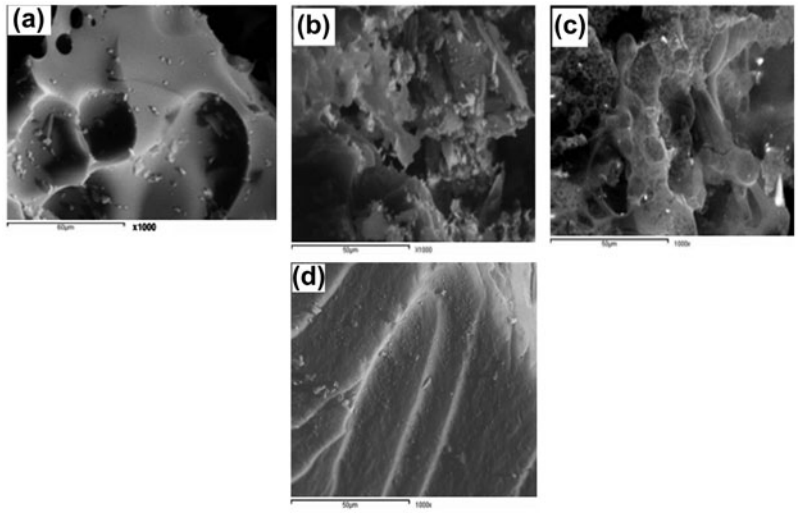

Fig. 3. SEM micrographs of ACXs prepared by chemical activation: (a) CX-MEA, (b) CX-HPO, (c) CX-KOH, and (d) as representative SEM for adsorption of methomyl on CX-HPO.

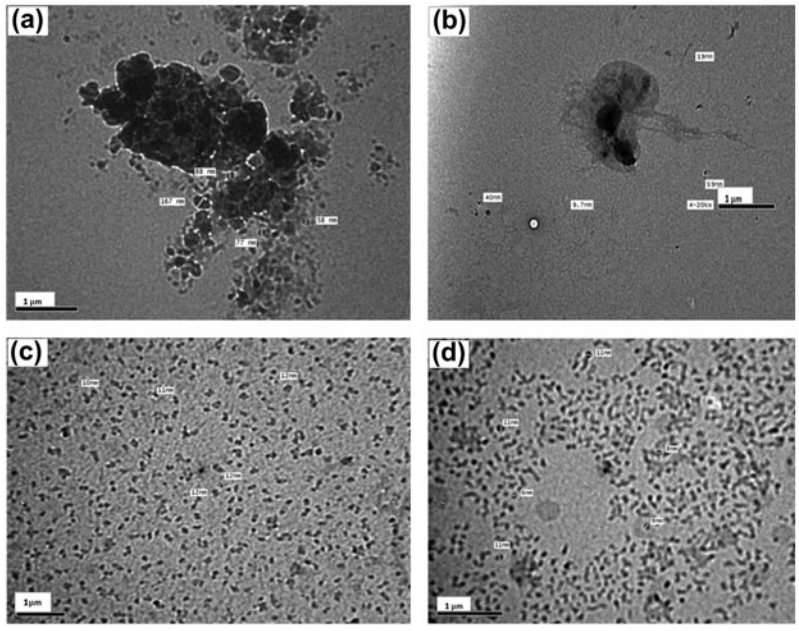

Fig. 4. TEM photographs of the (a) parent RFX, (b) CX-MEA, (c) CX-HPO, and (d) CX-KOH.

TEM displays a distinctive fine and nanosized spherical particles interconnected to form a three-dimensional network structure with irregular shape as in RFX and CX-MEA samples. The solid phase in parent RFX exhibits agglomerates of spherical particles with average diameter ranging from 58 to 167 nm which decreased to sizes between 10 and 59 nm, 10 and 12 nm, and 6 and 11 nm during chemical activation with MEA, H_3PO_4, and KOH, respectively. The spherical particles of CX-HPO and CX-KOH samples show a homogeneous distribution. Overall, the alkali activation with KOH seems to be the most effective activating agents in producing ACX adsorbent due to its high specific surface area and good surface chemistry, even though it was used in a small mass ratio of KOH to RFX precursor (1:1) [21,23].

3.4. Porosity development in prepared ACXs

Fig. 5 shows the N_2 adsorption–desorption isotherms at −196°C for the prepared carbon xerogels. It is clearly seen that the prepared carbons have different textural characteristics, confirming the significant effect of the chemical agents used in this study. The nitrogen isotherm curves for CX-HPO and CX-KOH samples show significant increase in the low relative pressure ($P/P^0 < 0.2$), indicating the presence of micropores in the prepared carbons with different extents.

The adsorption of nitrogen on the CX-MEA sample is the lowest as compared to the other carbons. It belongs to type II isotherm where the adsorption occurs on mixed micropores and opens surfaces with multilayer formation with a narrow hysteresis loop. This isotherm is typical for non-porous or meso–macroporous adsorbents. This result is confirmed by SEM micrograph of CX-MEA (Fig. 3), showing a creation of meso and macropores with few micropores on its surface, where $V_{micro} = 0.0155\ cm^3/g$ (Table 2).

However, the N_2 adsorption–desorption isotherms of CX-HPO and CX-KOH exhibited high nitrogen uptake at low relative pressure (P/P^0) and displayed a type IV isotherm according to BDDT classification

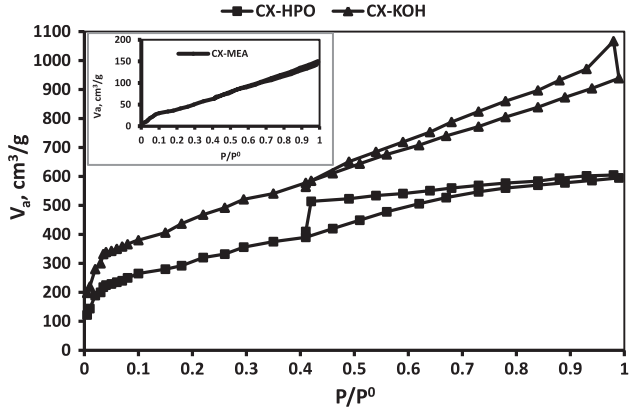

Fig. 5. Nitrogen adsorption–desorption isotherms of prepared ACXs.

with hysteresis loops of H2 and H4 [27], respectively. This finding attributed to the creation of mesoporous structure with open cylindrical pores associated with agglomerates of nanospherical particles as seen by TEM (Fig. 4) or ink-bottle pores, respectively. The hysteresis loop in nitrogen desorption for CX-HPO is observed in the P/P^0 range of 0.4–0.8 which is indicative of mesoporosity in the structure of the carbon in addition to the presence of micropores. However, in the case of CX-KOH, the hysteresis loop is shifted to a higher P/P^0 range (0.6–1.0), ascribing to the existence of mesopores with larger diameters in the structure. Thus, the activation of the parent RFX with H_3PO_4 and KOH (CX-HPO and CX-KOH) developed carbons with well-defined micro–mesoporous structure. It was observed that the mesoporosity in CX-KOH (52.5%) is higher than that formed in CX-HPO (34.6%), however, they are mostly microporous materials (microporosity about 57.5 and 65.4% in CX-KOH and CX-HPO, respectively). This porosity is known as interparticle porosity and originated from the spaces between the spherical particles of the original RFX during the chemical activation which indicates the presence of a bi-modal PSD (Fig. 6). This result was also reported earlier by Conceição et al. [22].

The textural characteristics (S_{BET}, S_{micro}, V_T, and V_{micro}) of the resulted ACXs are collected in Table 2. High values of surface area and total pore volume of 1,146 and 1,700 m^2/g, 0.9446 and 1.668 cm^3/g were determined for the carbon xerogels CX-HPO and CX-KOH, respectively, which are considerably higher than the one obtained for CX-MEA (212.2 m^2/g and 0.2236 cm^3/g). Also, in comparison to micropore and mesopore volumes (Table 2), the results clearly show that CX-KOH has much larger micropore and mesopore volumes than other samples obtained. It was found that the ratios of mesopore to micropore volumes are 13.4, 1.44, and 2.80 times for CX-MEA, CX-HPO, and CX-KOH, respectively. This interesting result showed that the monoethanol amine can be used as an effective chemical agent in producing highly developed meso–macroporous carbon materials with low microporosity equal to only 6.93% of total porosity. Thus, the trend in the V_T values as well as the shape of isotherm above relative pressure P/P^0 reflects the creating and/or widening of pores which is also visible in the SEM micrographs.

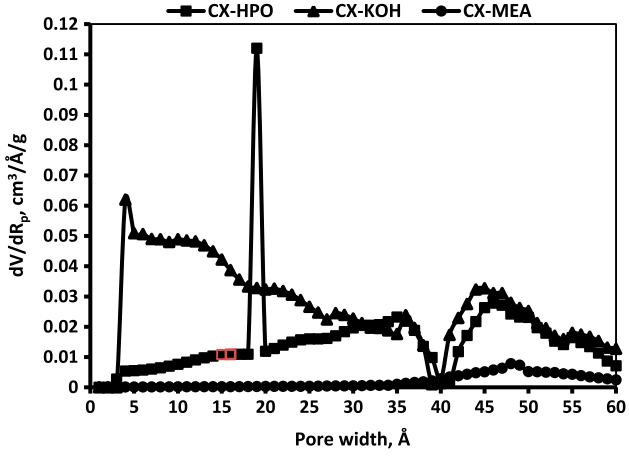

Fig. 6. PSD plots of the prepared ACXs.

Moreover, the high microporosity of the porous adsorbent was evident when comparing the micropore volume with the total pore volume. Table 2 also shows the ratios of micropore surface area to total surface area and micropore volume to total pore volume (S_{micro}:S_{BET} = 36.8–65.4% and V_{micro}:V_T = 6.90–40.9%) that reflect the distribution of the porosity on the surface of the resulted carbons. Apparently, the variation in the chemical agent activation of the parent RFX led to appreciable changes in these ratios, indicating that the PSDs are correlated with the chemical activation conditions adopted in this study. These changes corresponded to a shift in PSD between micropores and non-micropores (i.e. meso and macropores) as shown in Fig. 6.

Fig. 6 illustrates the plots of PSDs starting from 0 to 60 Å to describe the detail features of pore structures in the ACXs. The sharp PSDs were observed in the CX-HPO and CX-KOH samples, and the average pore diameters were different as expected from N_2 isotherms. The PSD of CX-MEA displays mono-modal peak of a wide pore range located between 30 and 59 Å, and the highest pore diameter centered at 31.7 Å. In the case of CX-HPO and CX-KOH samples, the PSD peaks show bi-modal peaks with the dominant pore diameters at around 19.3 and 4.17 Å, and another peak at 45 and 44 Å, respectively. This confirms that the carbons produced by H_3PO_4 or KOH activation exhibited micro–mesoporous structures with different extents, mostly containing ultra-micropores (<7 Å) in CX-KOH and super-micropores in CX-HPO (~7 Å).

Overall, the employed chemical agents used for RFX activation clearly play a definitive role in the development of porosity of the obtained ACXs.

3.5. Effects of pH and carbon dose

In liquid-phase adsorption, it is very important to identify the optimum adsorption pH since it affects not only the surface charge of the adsorbent, but also the degree of the ionization and speciation of

adsorbate during the adsorption process. According to the previous study [14], methomyl is quite stable in the pH range of 2–8, whereas at pH >8, it becomes unstable and degradable, thus the effect of pHon the uptake of methomyl using the prepared ACXs (CX-MEA, CX-HPO, and CX-KOH) was studied at pH values between 2 and 8 (Fig. 7(a)). The results indicated that the uptake of methomyl increases with increasing pH value up to 5 and then decreases over pH 5 for all tested ACXs. The CX-KOH exhibited higher uptake of methomyl at pH 5 as compared to other samples. The pH of the slurry of CX-KOH is 8.65 > 5 (pH of the solution), meaning that the surface of CX-KOH gets surrounded with positive charges and possesses highly positive sites, probably these enhance the uptake of methomyl on this sample. Thus, the adsorption of methomyl on the prepared carbons may be mainly attributed to the dispersion forces and polarization of π electrons present on methomyl [14]. In addition, the maximum uptake of methomyl occurred at pH 5 which corresponds to the initial pH of methomyl solution without any adjustment, making the adsorption process of this pollutant more attractive from the point of view of real application.

To assess the ability of the prepared carbons in promoting the adsorption of methomyl, the effect of carbon dose was employed by conducting experiments with 0.02, 0.05, 0.1, 0.2, and 0.5 g per 50 mL of 100 mg/L methomyl solution as shown in Fig. 7(b). It was found that the optimum carbon dose was 0.1 g carbon/50 mL methomyl (2 g/L) for all tested ACXs. On increasing the carbon dose from 0.1 to 0.5 g/mL, the uptake amount of methomyl is decreased gradually. This result may be due to the aggregation of carbon particles and hence led to a reduction in both the number of adsorption sites and consequently a decrease in the uptake of methomyl.

3.6. Adsorption studies of methomyl

To study the adsorption capacity of the prepared carbons, the removal of methomyl was carried out in batch experiments to describe the equilibrium adsorption using three classical adsorption isotherm models as follows [36–38]:

Langmuir isotherm model

$$\frac{C_e}{q_e} = \frac{1}{K_L Q_m} + \frac{1}{Q_m} C_e \tag{3}$$

Freundlich isotherm model

$$\ln\ q_e = \ln\ K_F + 1/n\ \ln\ C_e \tag{4}$$

Temkin isotherm model

$$q_e = B_1 \ln\ K_T + B_1 \ln\ C_e \tag{5}$$

where C_e is the equilibrium concentration of adsorbate (mg/L), q_e is the amount of methomyl adsorbed at equilibrium (mg/g), Q_m is the maximum adsorption capacity per unit weight of the adsorbent (mg/g), and K_L (L/mg) is the Langmuir adsorption equilibrium constant, where Q_m and K_L are calculated from the slope and intercept of the isotherm plot C_e/q_e vs. C_e. For Freundlich equation, K_F ((mg/g)/(L/mg)$^{1/n}$) is roughly an indicator of the adsorption capacity and $1/n$ is the adsorption intensity. Freundlich constants K_F and n can be calculated from the intercept and slope of the linear plot with ln q_e against ln C_e. In the case of Temkin equation, $B_1 = (RT/b)$ and K_T are the Temkin constants [38]. K_T is the equilibrium binding constant (L/mol) corresponding to the maximum binding energy, b is the variation of adsorption energy

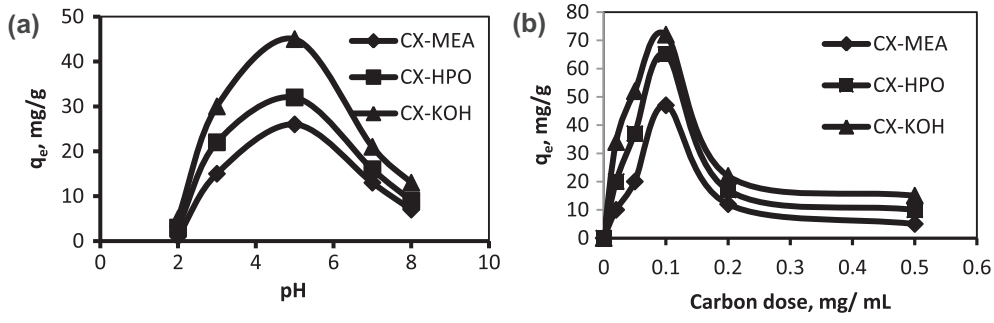

Fig. 7. Influence of (a) pH and (b) carbon dose on the adsorption of methomyl by ACXs (C_0 = 100 mg/L, T = 25°C, carbon dose = 0.1 g/50 mL, and contact time = 120 min).

(J/mol), and constant B_1 is related to the heat of adsorption. The Gibbs free energy, ΔG° (kJ/mol), for the adsorption process was obtained at 25°C ($\Delta G^\circ = -RT \ln K_L$ [38], where R is the universal gas constant at STP, 8.314 J/mol K, and T is the absolute temperature in Kelvin). Also, Table 3 lists surface density (mmol/m^2) which is known as the adsorbed amount of methomyl (mmol/g) as a function of the total surface area of ACX adsorbent (m^2/g) [20].

The model parameters and their corresponding regression coefficients (r^2) are listed in Table 3. In the range of tested concentrations, Langmuir (r^2 = 0.989–0.999) and Temkin models (r^2 = 0.947–0.977) fit the adsorption data well, while Freundlich model (r^2 = 0.912–0.936) shows lower correlation with the experimental adsorption data. Fig. 8 presents the adsorption isotherm curves of methomyl onto the prepared ACXs, showing L-type isotherms for adsorption of pesticide by all the prepared carbons. Results of regression coefficients show that the Langmuir and Temkin models are globally best fitted with the equilibrium data of methomyl adsorption, confirming that there are electrostatic interactions occurred in the adsorption process. As shown in Table 3, the maximum adsorption capacity values were 15.2, 52.4, and 125 mg/g for methomyl adsorbed onto the prepared carbons CX-MEA, CX-HPO, and CX-KOH, respectively, although the higher values of K_L = 0.1778 and r^2 = 0.999 appeared with CX-MEA, confirming that the monolayer adsorption of methomyl was more favored (isotherm of L-type).

In addition, the essential features of Langmuir adsorption isotherm can be expressed in terms of a dimensionless separation factor (R_L), which is given by equation:

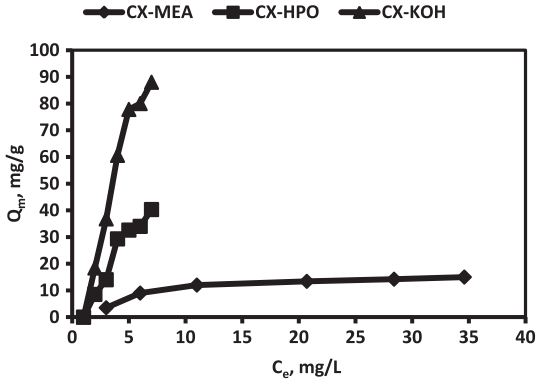

Fig. 8. Adsorption isotherms of methomyl on the prepared ACXs (C_0 = 20–100 mg/L, T = 25°C, carbon dose = 0.1 g/50 mL, and contact time = 24 h).

$$R_L = \frac{1}{1 + C_0 K_L} \tag{6}$$

where C_0 is the initial concentration of methomyl (mg/l). The R_L value indicates the shape of the isotherm as follows: irreversible (R_L = 0), favorable (0 < R_L <1), linear (R_L = 1), or unfavorable isotherm (R_L > 1). Also, R_L values are represented in Table 3, which confirmed that the prepared carbons are highly favorable for adsorption of methomyl from wastewater under the reported conditions used in this study. The negative value of Gibbs free energy (ΔG°=−24.8 to −27.7 kJ/mol) confirms the feasibility and spontaneous nature of the adsorption of methomyl onto the tested carbons.

Recently, in comparison to other porous adsorbents used for removing methomyl pesticide from aqueous solution, Chang et al. studied the adsorptive removal of the methomyl pesticide using hypercrosslinked polymers Macronet (MN-100) [14], MN-150 and MN-500) [15]. They found that, the maximum adsorption capacity for methomyl was found to be 21.6 mg/g onto MN-100, 0.04 and 0.005 mg/g onto MN-150, and MN-500 adsorbents, respectively. Chang and Lee [4] also reported the adsorption behavior of methomyl on a commercial activated carbon (F400) using a high gravity rotating packed bed reactor (HGRPBR) system to promote the adsorption process. El-Geundi et al. [16] carried out equilibrium experiments for adsorption of methomyl using activated carbon prepared by chemical activation of cotton stalks with KOH at 500°C for 2 h. They found that the maximum adsorption capacity was 72.8 mg/g at 25°C. From the abovementioned studies, it can be concluded that the CX-KOH prepared ACX has the highest adsorption capacity (Q_m = 125 mg/g).

Regarding the kinetic studies of methomyl adsorption, experiments were carried out to understand the behavior of adsorption onto the prepared carbon adsorbent. The controlling mechanisms of adsorption processes were investigated according to usual global kinetic expressions such as pseudo-first-order, pseudo-second-order, and intraparticle diffusion kinetic models [38,39].

Pseudo-first-order equation

$$\log (q_e - q_t) = \log q_e - \frac{k_1 t}{2.303} \tag{7}$$

Pseudo-second-order equation

$$t/q_t = \frac{1}{k_2 {q_e}^2} + \frac{t}{q_e} \tag{8}$$

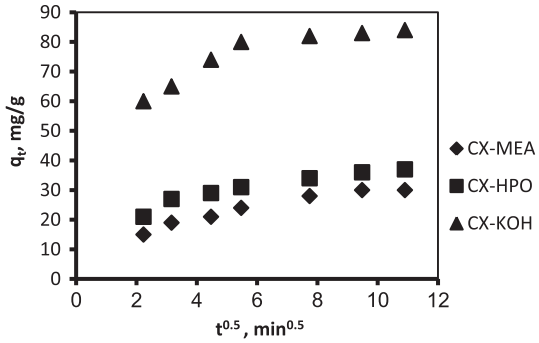

Fig. 9. Intraparticle diffusion plots for adsorption of methomyl onto prepared ACXs (C_0 = 20–100 mg/L, T = 25°C, carbon dose = 0.1 g/50 mL, and contact time = 120 min).

Intraparticle diffusion equation

$$q_t = k_{in}\, t^{1/2} + C_i \quad (9)$$

where q_t are the amounts of methomyl adsorbed at time t (min), k_1 is the equilibrium rate constant of pseudo-first-order sorption (min^{-1}), k_2 is the equilibrium rate constant of pseudo-second-order adsorption (g/mg min), and kqe^2 is the initial adsorption rate ($h = kqe^2$, mg/g min). Whereas k_{in} is the rate constant for intraparticle diffusion (mg/g $min^{0.5}$) which is calculated from the slope of the linear portion of q_t–$t^{1/2}$ plot, $t^{1/2}$ is the square root of the time, C_i is the intercept at stage i, where the value of C_i is related to the thickness of the boundary layer. The calculated values of the model parameters are given in Table 4. Also, Table 4 lists the regression coefficients of the linear form of model (r^2), which are a measure of the model satisfactory, indicating that the pseudo-second-order model (r^2 = 0.998–0.999) can adequately describe the adsorption data better than that of the pseudo-first-order model.

Table 3
Adsorption parameters of Langmuir, Freundlich, and Temkin isotherm models for removal of methomyl by the prepared ACXs

	ACXs adsorbents		
Equilibrium models	CX-MEA	CX-HPO	CX-KOH
Langmuir			
Q_m (mg/g)	15.2	52.3	125
Q_m (mmol/g)	0.0934	0.3227	0.7706
K_L (L/mg)	0.1778	0.1392	0.4444
R_L	0.0532	0.0670	0.0220
ΔG° (kJ/mol)	−25.4	−24.8	−27.7
SD (mmol/m^2)[a]	2.65	1.69	2.73
r^2	0.999	0.998	0.989
Freundlich			
K_F (mg/g)/(L/mg)$^{1/n}$	3.09	7.21	32.9
$1/n$	0.4815	0.6417	0.5650
r^2	0.912	0.936	0.922
Temkin			
b (J/mol)	275.4	83.1	40.9
K_T (L/mol)	1.48	1.22	4.34
r^2	0.972	0.947	0.977

[a]SD is the surface density of adsorbent occupied by one molecule $\left[\mathrm{SD} = \frac{Q_m\ (\mathrm{mmol/g}) \times 6.023 \times 10^{23} \times 10^{-20}}{S_{BET}}\right]$.

The calculated adsorption capacity (q_e) values estimated by the pseudo-second-order model for removal of methomyl over CX-MEA, CX-HPO, and CX-KOH were 16.8, 32.2, and 85.5 mg/g, respectively, which is in accordance with the values measured experimentally (15.8, 33.8, and 88 mg/g, respectively). Therefore, the pseudo-second-order kinetic model was better fitted with the experimental data at high initial concentration (C_0 = 100 mg/L) based on the assumption that the rate-limiting step involves chemisorptions [36]. The adsorption of methomyl by CX-KOH showed higher values of pseudo-second-order constant (k_2)

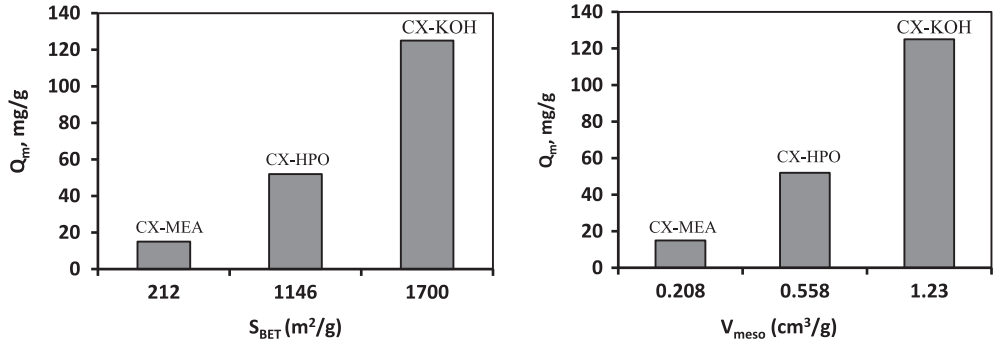

Fig. 10. Correlation between the adsorption capacity (Q_m, mg/g) for methomyl with total specific surface area (S_{BET}, m^2/g) and mesopore volume (V_{meso}, cm^3/g).

Table 4
Parameters of kinetic models for adsorption of methomyl by the prepared ACXs (C_0 = 100 mg/L, volume = 100 mL, pH 5, carbon dose = 0.1 g/50 mL, contact time = 120 min, and T = 25°C)

	Pseudo-first-order kinetic			Pseudo-second-order kinetic				Intraparticle diffusion	
Samples	q_e (mg/g)	k_1 (min^{-1})	r^2	q_e (mg/g)	k_2 (g/mg min)	h (mg/g min)	r^2	k_{in} (mg/g $min^{0.5}$)	C_i
CX-MEA	81.9	1.61×10^{-3}	0.848	16.8	3.83×10^{-3}	3.96	0.998	1.72	13.2
CX-HPO	60.6	1.84×10^{-3}	0.806	32.2	4.86×10^{-3}	7.08	0.999	1.61	20.7
CX-KOH	32.8	7.14×10^{-3}	0.745	85.5	0.012	31.8	0.999	2.61	59.2

and initial rate (h) than those of methomyl adsorption on CX-HPO and CX-MEA.

Values of k_{in} and C_i can be determined from the slope and the intercept of the intraparticle diffusion plots, respectively. The intercept value reflects the importance of the boundary layer thickness, that is, the larger the intercept, the greater the thickness of the boundary layer. The intraparticle diffusion plots for adsorption of methomyl presented two stages (Fig. 9), where the straight line did not pass through the origin indicating that two steps have taken place due to the difference in mass transfer rate between initial and final adsorptions. The first stage (below 30 min) is the instantaneous or external surface adsorption, that is, the diffusion of the adsorbate through the solution to the external surface of the absorbent [37,40]. The second stage (over 30 min) is the phase of gradual adsorption where intraparticle diffusion is the rate-controlling step. From these results, it can be stated that the intraparticle diffusion is not solely responsible for the rate controlling. Anyway, the prepared CX-KOH showed higher values of k_{in} and C_i as compared to those evaluated for adsorption of methomyl by CX-MEA and CX-HPO samples.

3.7. Correlation between the adsorption capacity and porosity of ACXs

Fig. 10 shows the adsorption capacities of methomyl as a function of total specific surface area (S_{BET}, m^2/g) and mesopore volume (V_{meso}, cm^3/g) of the prepared carbons (Tables 2 and 3). Clearly, the adsorption capacity increased sharply with the increase in the surface area and mesopore volume, in addition to the presence of highly micropore volumes in both CX-HPO and CX-KOH samples (Table 2). This result indicates that the adsorption capacity for methomyl depends mainly on the total surface area and micro/mesopore size distributions. Moreover, the higher adsorption performance of CX-KOH compared to the other materials may be explained by the presence of basic oxygen functional groups present on the surface due to the alkaline chemical activation. This type of activation involves the reduction of the carbon atoms and the removal of the H and O atoms, with potassium-forming alkaline groups, such as –OK groups, causing the separation of carbon and the generation of a porous structure [41], resulting in a material with high specific surface area [42].

4. Conclusions

In this study, novel carbon adsorbents of nanosized spherical particles and tailored porous structure were prepared by chemical activation schemes from RFX using monoethanol amine, H_3PO_4, and KOH agents, respectively. The chemically ACXs can be used effectively for the removal of methomyl pesticide by adsorption from aqueous solution. The Langmuir and Temkin isotherm models showed a satisfactory fit with the methomyl adsorption onto the prepared ACXs. Maximum monolayer adsorption capacities of 15.2, 52.3, and 125 mg/g for methomyl adsorption onto CX-MEA, CX-HPO, and CX-KOH, respectively, were obtained at pH 5 and 25°C. Furthermore, the adsorption mechanism followed the pseudo-second-order kinetic model, suggesting that the adsorption rate is dependent more on the availability of adsorption sites in addition to the total surface area and mesopore size distribution. Finally, it can be concluded that the activation of RFX with KOH successfully produced a micro–mesoporous ACX with considerable nanosized particles (6–11 nm), and higher surface area and pore volume of 1,700 m^2/g and 1.668 cm^3/g, respectively, revealing superior performance toward removal of methomyl as compared to the other adsorbents reported in the literature [4,14–16].

Acknowledgments

The authors highly appreciate thoughtful and constructive review of Prof. Helder T. Gomes, Department

of Chemical and Biological Technology, School of Technology and Management, Bragança Polytechnic Institute, Campus Santa Apolónia, 5301-857 Bragança, Portugal.

References

[1] F.P. Carvalho, Agriculture, pesticides, food security and food safety, Environ. Sci. Policy 9 (2006) 685–692.

[2] Environmental Agency, The Annual Report of the Environmental Agency Pesticide, Monitoring Program, Environmental Agency, UK, 2002.

[3] R.A. Rebich, R.H. Coupe, E.M. Thurman, Herbicide concentrations in the Mississippi River Basin-the importance of chloroacetanilide herbicide degradates, Sci. Total Environ. 321 (2004) 189–199.

[4] C. Chang, S. Lee, Adsorption behavior of pesticide methomyl on activated carbon in a high gravity rotating packed bed reactor, Water Res. 46 (2012) 2869–2880.

[5] W.J. Hayes Jr., E.R. Laws Jr. (Eds.), Handbook of Pesticide Toxicology. Classes of Pesticides, vol. 3, Academic Press, Inc., New York, NY, 1991, p. 1165.

[6] US Environmental Protection Agency (EPA), Reregistration Eligibility Decision (RED), Facts-Methomyl, EPA-738-F-98-019, Preventation, Pesticides and Toxic substances (1998).

[7] Extoxnet Pesticide Information Profiles (PIPs). Available from: <http://extoxnet.orst.edu/pips/ghindex.html>, As posted on July 26, 2007, is a cooperative effort of University of California-Davis, Oregon State University, Michigan State University, Cornell University, and the University of Idaho.

[8] M. Farré, J. Fernandez, M. Paez, L. Granada, L. Barba, H.M. Gutierrez, C. Pulgarin, D. Barceló, Analysis and toxicity of methomyl and ametryn after biodegradation, Anal. Bioanal. Chem. 373 (2002) 704–709.

[9] H. Börner, Pesticides in Ground and Surface Water in Chemistry of Plant Protection, Spring-Verlag GmbH, Berlin, Germany, 1994.

[10] K. Ignatowicz, Selection of sorbent for removing pesticides during water treatment, J. Hazard. Mater. 169 (2009) 953–957.

[11] A. Jusoh, W.J. Hartini, N. Ali, A. Endut, Study on the removal of pesticide in agricultural run off by granular activated carbon, Bioresour. Technol. 102 (2011) 5312–5318.

[12] R. Li, C. Yang, H. Chen, G. Zeng, G. Yu, J. Guo, Removal of triazophos pesticide from wastewater with Fenton reagent, J. Hazard. Mater. 167 (2009) 1028–1032.

[13] B.H. Hameed, J.M. Salman, A.L. Ahmad, Adsorption isotherm and kinetic modeling of 2,4-D pesticide on activated carbon derived from date stones, J. Hazard. Mater. 163 (2009) 121–126.

[14] C.-F. Chang, C.-Y. Chang, K.-E. Hsu, W. Höll, P.-C. Chiang, Removal of methomyl pesticide by adsorption using novel hypercrosslinked polymer of macronet MN-100, J. Environ. Eng. Manage. 17 (2007) 311–318.

[15] C.-F. Chang, C.-Y. Chang, K.-E. Hsu, S.-C. Lee, Adsorptive removal of the pesticide methomyl using hypercrosslinked polymers, J. Hazard. Mater. 155 (2008) 295–304.

[16] M.S. El-Geundi, M.M. Nassar, T.E. Farrag, M.H. Ahmed, Methomyl adsorption onto cotton stalks activated carbon (CSAC): Equilibrium and process design, Proc. Environ. Sci. 17 (2013) 630–639.

[17] E.J. Zanto, S.A. Al-Muhtaseb, J.A. Ritter, Sol−gel-derived carbon aerogels and xerogels: Design of experiments approach to materials synthesis, Ind. Eng. Chem. Res. 41 (2002) 3151–3162.

[18] B.S. Girgis, A.A. Attia, N.A. Fathy, Potential of nanocarbon xerogels in the remediation of dye-contaminated water discharges, Desalination 265 (2011) 169–176.

[19] A.M. El-Khatat, S.A. Al-Muhtaseb, Advances in tailoring resorcinol-formaldehyde organic and carbon gels, Adv. Mater. 23 (2011) 2887–2903.

[20] B.S Girgis, I.Y. El-Sherif, A.A. Attia, N.A. Fathy, Textural and adsorption characteristics of carbon xerogel adsorbents for removal of Cu(II) ions from aqueous solution, J. Non-Cryst. Solids 358 (2012) 741–747.

[21] B.S. Girgis, M.N. Alaya, I.Y. El-Sherif, A.A. Attia, N.A. Fathy, Development of porosity and copper(II) ion adsorption capacity by activated nano-carbon xerogels in relation to treatment schemes, Adsorpt. Sci. Technol. 29 (2011) 943–962.

[22] F.L. Conceição, P.J.M. Carrott, M.M.L. Ribeiro Carrott, New carbon materials with high porosity in the 1–7 nm range obtained by chemical activation with phosphoric acid of resorcinol-formaldehyde aerogels, Carbon 47 (2009) 1874–1877.

[23] L. Zubizarreta, A. Arenillas, J.-P. Pirard, J.J. Pis, N. Job, Tailoring the textural properties of activated carbon xerogels by chemical activation with KOH, Microporous Mesoporous Mater. 115 (2008) 480–490.

[24] R.S. Ribeiro, N.A. Fathy, A.A. Attia, A.M.T. Silva, J.L. Faria, H.T. Gomes, Activated carbon xerogels for the removal of the anionic azo dyes Orange II and Chromotrope 2R by adsorption and catalytic wet peroxide oxidation, Chem. Eng. J. 195–196 (2012) 112–121.

[25] M.A. Elsayed, P.J. Hall, M.J. Heslop, Preparation and structure characterization of carbons prepared from resorcinol-formaldehyde resin by CO_2 activation, Adsorption 13 (2007) 299–306.

[26] H.P. Boehm, Surface oxides on carbon and their analysis: A critical assessment, Carbon 40 (2002) 145–149.

[27] K.S.W. Sing, D.H. Everett, R.A.W. Haul, L. Moscou, R.A. Pierotti, J. Rouquerol, T. Siemieniewska, Reporting physisorption data for gas solid systems with special reference to the determination of surface-area and porosity, (recommendations 1984), Pure Appl. Chem. 57 (1985) 603–619.

[28] W.D. Harkins, G. Jura, Surfaces of solids. XIII. A vapor adsorption method for the determination of the area of a solid without the assumption of a molecular area, and the areas occupied by nitrogen and other molecules on the surface of a solid, J. Am. Chem. Soc. 66 (1944) 1366–1373.

[29] R.J. Dombrowski, D.R. Hyduke, C.M. Lastoskie, Pore size analysis of activated carbons from argon and nitrogen porosimetry using density functional theory, Langmuir 16 (2000) 5041–5050.

[30] C.A. Leon y Leon, J. Solar, V. Calemma, L. Radovic, Evidence for the protonation of basal plane sites on carbon, Carbon 30 (1992) 797–811.

[31] E. Fuente, J.A. Menéndez, D. Suárez, M.A. Montes-Morán, Basic surface oxides on carbon materials: A global view, Langmuir 19 (2003) 3505–3511.
[32] J.B. Lambert, Organic Structural Spectroscopy, Prentice Hall, Upper Saddle River, New Jersey, 1998.
[33] G.H. Oh, C.H. Yun, C.R. Park, Role of KOH in the one-stage KOH activation of cellulosic biomass, Carbon Sci. 4 (2003) 180–184.
[34] S. Bashkova, T.J. Bandosz, The effects of urea modification and heat treatment on the process of NO_2 removal by wood-based activated carbon, J. Colloid Interface Sci. 333 (2009) 97–103.
[35] M. Jagtoyen, F. Derbyshire, Activated carbons from yellow poplar and white oak by H_3PO_4 activation, Carbon 36 (1998) 1085–1097.
[36] X.L. Han, W. Wang, X.J. Ma, Adsorption characteristics of methylene blue onto low cost biomass material lotus leaf, Chem. Eng. J. 171 (2011) 1–8.
[37] B.S. Inbaraj, K. Selvarani, N. Sulochana, Evaluation of a carbonaceous sorbent prepared from Pearl Millet Husk for its removal of basic dyes, J. Sci. Ind. Res. 61 (2002) 971–978.
[38] N.A. Fathy, O.I. El-Shafey, L.B. Khalil, Effectiveness of alkali-acid treatment in enhancement the adsorption capacity for rice straw: The removal of methylene blue dye, ISRN Phys. Chem. 2013 (2013) 1–15.
[39] W.J. Webeer, J.C. Morris, Kinetics of adsorption of carbon from solution, J. Sanitary Eng. Div.-ASCE 89 (1963) 31–59.
[40] Z. Li, P.-H. Chang, J.-S. Jean, W.-T. Jiang, C.-J. Wang, Interaction between tetracycline and smectite in aqueous solution, J. Colloid Interface Sci. 341 (2010) 311–319.
[41] J. Li, J. Li, Y.Q. Lai, H.S. Song, Z.A. Zhang, Y.X. Liu, Influence of KOH activation techniques on pore structure and electrochemical property of carbon electrode materials, J. Central South Univ. Technol. 13 (2006) 360–366.
[42] E. Raymundo-Piñero, P. Azaïs, T. Cacciaguerra, D. Cazorla-Amorós, A. Linares-Solano, F. Béguin, KOH and NaOH activation mechanisms of multiwalled carbon nanotubes with different structural organisation, Carbon 43 (2005) 786–795.